Superconductivity in Pristine $2H_a$-MoS$_2$ at Ultrahigh Pressure

Zhenhua Chi,[1] Xuliang Chen,[2] Fei Yen,[1] Feng Peng,[3] Yonghui Zhou,[2] Jinlong Zhu,[4] Yijin Zhang,[5] Xiaodi Liu,[1]
Chuanlong Lin,[6] Shengqi Chu,[7] Yanchun Li,[7,*] Jinggeng Zhao,[8,9,†] Tomoko Kagayama,[10]
Yanming Ma,[11] and Zhaorong Yang[1,2,12,‡]

[1]*Key Laboratory of Materials Physics, Institute of Solid State Physics, Chinese Academy of Sciences,
Hefei 230031, People's Republic of China*
[2]*Anhui Province Key Laboratory of Condensed Matter Physics at Extreme Conditions, High Magnetic Field Laboratory,
Chinese Academy of Sciences, Hefei 230031, People's Republic of China*
[3]*College of Physics and Electronic Information, Luoyang Normal University,
Luoyang 471022, People's Republic of China*
[4]*Center for High Pressure Science and Technology Advanced Research (HPSTAR), Beijing 100094,
People's Republic of China*
[5]*Max Planck Institute for Solid State Research, Stuttgart 70569, Germany*
[6]*Center for High Pressure Science and Technology Advanced Research (HPSTAR),
Shanghai 201203, People's Republic of China*
[7]*Multidiscipline Research Center, Institute of High Energy Physics, Chinese Academy of Sciences,
Beijing 100049, People's Republic of China*
[8]*Department of Physics, Harbin Institute of Technology, Harbin 150080, People's Republic of China*
[9]*Natural Science Research Center, Academy of Fundamental and Interdisciplinary Sciences,
Harbin Institute of Technology, Harbin 150080, People's Republic of China*
[10]*KYOKUGEN, Center for Science and Technology under Extreme Conditions, Graduate School of Engineering Science,
Osaka University, 1-3 Machikaneyama, Toyonaka, Osaka 560-8531, Japan*
[11]*State Key Laboratory of Superhard Materials, College of Physics, Jilin University,
Changchun 130012, People's Republic of China*
[12]*Collaborative Innovation Center of Advanced Microstructures,
Nanjing University, Nanjing 210093, People's Republic of China*

As a follow-up of our previous work on pressure-induced metallization of the $2H_c$-MoS$_2$ [Chi *et al.*, Phys. Rev. Lett. **113**, 036802 (2014)], here we extend pressure beyond the megabar range to seek after superconductivity via electrical transport measurements. We found that superconductivity emerges in the $2H_a$-MoS$_2$ with an onset critical temperature T_c of ca. 3 K at ca. 90 GPa. Upon further increasing the pressure, T_c is rapidly enhanced beyond 10 K and stabilized at ca. 12 K over a wide pressure range up to 220 GPa. Synchrotron x-ray diffraction measurements evidenced no further structural phase transition, decomposition, and amorphization up to 155 GPa, implying an intrinsic superconductivity in the $2H_a$-MoS$_2$. DFT calculations suggest that the emergence of pressure-induced superconductivity is intimately linked to the emergence of a new flat Fermi pocket in the electronic structure. Our finding represents an alternative strategy for achieving superconductivity in $2H$-MoS$_2$ in addition to chemical intercalation and electrostatic gating.

With the advent of the graphene race, two-dimensional transition metal dichalcogenides (TMDs) have gained reinvigorated attention due to their exotic properties such as indirect-direct band gap crossover [1], valley polarization [2], quantum spin Hall effect [3], and Ising superconductivity [4]. Layered TMDs with the chemical formula MX_2 (M = Ti, Nb, Ta, Mo, W; X = S, Se, Te) share a common structural motif of X-M-X sandwich, but exhibit a wide variety of polymorphs such as T_d, $1T$, $1T'$, $2H$, and $3R$, differing in the number of X-M-X sandwich per unit cell and the coordination of the MX_6 polyhedron [5]. In terms of the electronic ground state, a charge-density

wave (CDW) generally competes with superconductivity in TMDs [6]. At ambient pressure, superconductivity has been observed in semimetallic T_d-MoTe$_2$ [7], metallic $2H$-NbS$_2$, $2H$-NbSe$_2$, $2H$-TaS$_2$, and $2H$-TaSe$_2$. In addition, superconductivity can be induced by charge-carrier doping via either chemical intercalation [8–10] or electrostatic gating [11–14] in all polymorphs.

Pressure is a viable physical tuning parameter in modifying the crystal structure along with related band structure of a crystalline material in a clean and controllable manner without introducing chemical disorder [15–17]. It has been routinely observed in the CDW-bearing $1T$ polymorph of

TMDs [18,19], heavy fermions, and organic salts that superconductivity emerges when the CDW or spin-density wave (SDW) state is suppressed by pressure. The generic pressure-temperature (P-T) phase diagram featured by a superconductivity dome in the vicinity of an ordered state implies an unconventional pairing mechanism mediated by the critical fluctuations of the nearby ordered state. Pressure-induced superconductivity has also been observed in the semimetallic CDW-free T_d polymorph of TMDs [20,21]. However, the definitive evidence for pressure-induced superconductivity in the semiconducting CDW-free $2H$ polymorph of TMDs remains absent so far. $2H$-MoS$_2$ is such an archetypal semiconductor with an indirect (direct) band gap of 1.3 (1.9) eV at ambient pressure. Upon compression, the $2H_c$-MoS$_2$ undergoes a $2H_c$-to-$2H_a$ polytype transformation accompanied by a semiconductor-to-metal transition via band overlap at ca. 25 GPa. No marked signature of superconductivity was observed at pressures up to 80 GPa [22,23]. By further increasing the pressure to beyond 100 GPa, we report in this Letter the first observation of superconductivity in the $2H_a$-MoS$_2$.

Single crystals of the $2H_c$-MoS$_2$ were grown by conventional chemical vapor transport [24]. The standard four-point probe electrical transport measurements were carried out using a screw-pressure-type diamond anvil cell (DAC) made of non-magnetic Cu-Be alloy in a homemade multifunctional measurement system (1.8–300 K, JANIS Research Company Inc.; 0-9 T, Cryomagnetics Inc.). Two runs of high pressure synchrotron x-ray diffraction measurements were conducted on the beam line of Advanced Photon Source. DFT calculations were performed to complement the experiments. Details about the high-pressure measurements and DFT calculations can be found in the Supplemental Material [25], which includes Refs. [26–34].

Figure 1 shows the temperature-dependent resistance $R(T)$ of the $2H_a$-MoS$_2$ at pressures from 30 to 220 GPa in three runs. As displayed in Fig. 1(a), the $R(T)$ at 30 GPa exhibits a broad hump centered ca. 270 K, which becomes less pronounced with pressure and disappears completely at 60 GPa. This anomaly is likely caused by the formation of pressure-induced CDW, as will be discussed below. Upon increasing the pressure to 70 GPa, the $R(T)$ is characteristic of a metal over the whole temperature range studied. Interestingly, superconductivity characterized by a precipitous drop in the $R(T)$ sets in at pressures above 100 GPa, as shown in Fig. 1(b). The superconducting transition critical temperature T_c defined here as the onset of the resistance drop, indicated in Fig. 2(a), is enhanced from 5 K at 100 GPa to 10 K at 115 GPa and to 11 K at 125 GPa. T_c remains nearly constant at 11.5 K over a wide pressure range from 135 to 180 GPa, eventually rises to 12 K at 200 GPa. At the highest pressure of 220 GPa in the present study, the normalized resistance of $R(1.7\ \mathrm{K})/R(15\ \mathrm{K})$
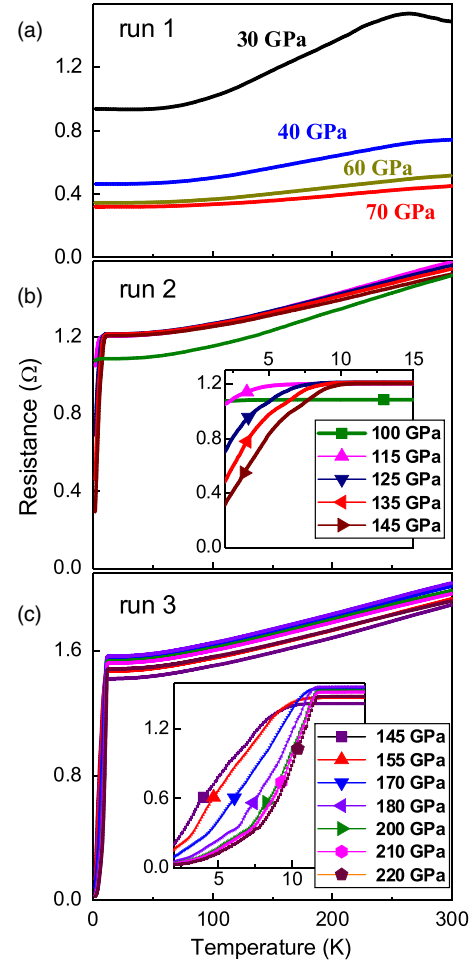

FIG. 1. Temperature-dependent resistance of $2H_a$-MoS$_2$ at elevated pressures. (a) R-T curves at pressures between 30 and 70 GPa in run 1. (b) R-T curves at pressures between 100 and 145 GPa in run 2. (c) R-T curves at pressures between 145 and 220 GPa in run 3. The inset in (b) and (c) is the close-up of the low-temperature region, highlighting the superconducting transition.

approaches a vanishingly small value of 0.017 with a residual resistance of ∼25 mΩ at 1.7 K. It is likely that a pressure gradient throughout the sample due to a non-hydrostatic pressure condition [35,36] broadens the superconducting transition and gives rise to a nonzero resistance in the superconducting state.

The presence of pressure-induced superconductivity in the $2H_a$-MoS$_2$ is further corroborated by the resistance measurements under external magnetic fields. Figure 2(a) displays the $R(T)$ at 220 GPa under various magnetic fields up to 6.5 T applied along the c axis of the crystal. As can be seen, T_c is clearly suppressed to lower temperatures with increasing magnetic field, typical for a bulk superconducting transition. Figure 2(b) displays the upper critical field $\mu_0 H_{c2}$ as a function of critical temperature T_c. The zero-temperature $\mu_0 H_{c2}(0)$ can be estimated to be 7.5 T (orbital limit) and 8.1 T by fitting the $\mu_0 H_{c2}(T)$
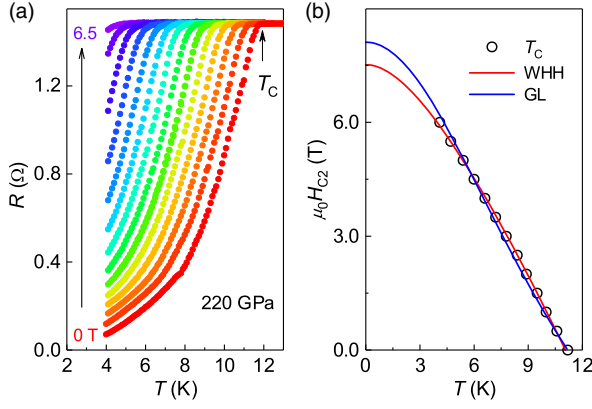
FIG. 2. The determination of zero-temperature upper critical magnetic field $\mu_0 H_{c2}(0)$ of $2H_a$-MoS$_2$ at 220 GPa. (a) R-T curves under external magnetic fields of up to 6.5 T at steps of 0.5 T. (b) $\mu_0 H_{c2}$-T phase diagram. The solid line in red and blue represents fitting by the WHH formula and GL equation, respectively.

FIG. 3. Pressure-temperature (P-T) phase diagram of $2H$-MoS$_2$. The vertical dashed line demarcates the boundary between the semiconducting and metallic states. The inset displays the T^3 linear dependence of R following the equation of $R(T) = R_0 + AT^n$ with $n = 3(\pm 0.2)$ over the temperature range from T_c up to 50 K at 220 GPa, where R_0 is the residual resistance and A is the thermal coefficient. The error bar on T_c indicates the uncertainty due to pressure gradient. The error bar on pressure indicates 95% confidence interval.

with the conventional one-band Werthamer-Helfand-Hohenberg (WHH) formula for an isotropic s-wave superconductor [37] and the Ginzburg-Landau (GL) equation [38], respectively. Both $\mu_0 H_{c2}(0)$ values are lower than the Bardeen-Cooper-Schrieffer (BCS) weak-coupling Pauli paramagnetic limit of $\mu_0 H_p = 1.84 T_c = 22$ T for $T_c = 12$ K, but higher than that of the superconductivity achieved via either chemical intercalation or electrostatic gating. The Pauli limiting field is determined by the Zeeman energy required to break the Cooper pairs. It is likely that the strong spin-orbit coupling (SOC) contribution to superconductivity characterized by the quasilinear temperature dependence of $\mu_0 H_{c2}$ might strengthen the Pauli paramagnetic pair breaking within the WHH framework [37]. The validity of the Pauli limiting field implies a phonon-mediated superconductivity in the $2H_a$-MoS$_2$. In addition, the upward curvature of $\mu_0 H_{c2}(T_c)$ close to the zero-field limit hints at a possible multiband superconducting pairing state, reminiscent of $2H$-NbS$_2$, $2H$-NbSe$_2$, and MgB$_2$ [39–41].

The pressure-temperature (P-T) phase diagram of $2H$-MoS$_2$ is shown in Fig. 3. At pressures below ca. 25 GPa, $2H_c$-MoS$_2$ is a semiconductor. At ca. 25 GPa, a semiconductor-to-metal transition accompanied by a $2H_c$-to-$2H_a$ polytype transformation takes place. At 40 GPa, the polytype transformation is completed. At pressures above 40 GPa, the pure metallic $2H_a$-MoS$_2$ is stabilized. Superconductivity emerges at ca. 90 GPa, and exhibits an extended superconducting region with a nearly pressure-independent T_c starting from above 135 GPa. Such a unique feature of $T_c(P)$ is characteristic of band overlap metallization of layered systems, in which the nearly two-dimensional electronic density of states (DOS) at the Fermi level [$N(E_F)$] is independent of the charge-carrier concentration. The P-T phase diagram of $2H_a$-MoS$_2$

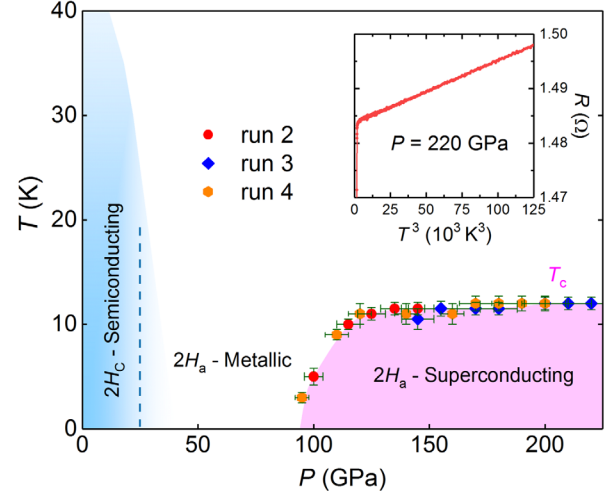differs from that of $1T$-TiSe$_2$ [18] and T_d-WTe$_2$ [21] with a superconducting dome, but resembles that of $1T$-TaS$_2$ [19] and Bi$_2$Se$_3$ [42]. For $1T$-TaS$_2$, the textured CDW phase that hosts superconductivity is characterized by a commensurability-driven and Coulombically frustrated electronic phase separation with the formation of domains. The superconductivity developed in the metallic interdomain regions is rather insensitive to pressure, giving rise to the pressure-independent T_c. For Bi$_2$Se$_3$, the pressure-independent T_c has been attributed to the delicate balance between the volume-dependent T_c through the phonon cutoff frequency $\langle \omega_c \rangle$ and the $N(E_F)$, as given by the BCS relationship and the McMillan strong-coupling formalism, respectively [43,44]. As shown in the inset of Fig. 3, the low-temperature normal-state resistance at 220 GPa exhibits a non-Fermi-liquid behavior, indicated by a power law fitting of $R(T) = R_0 + AT^n$ with $n = 3(\pm 0.2)$ over the temperature range from T_c up to 50 K, where R_0 is the residual resistance, A is the thermal coefficient and n is the temperature exponent. It is noteworthy to highlight that the fitted value of n retains a value close to 3 over a wide pressure range from 100 GPa up to 220 GPa. The fitted value of n is different from the expected value of $n = 2$ for electron-electron or $n = 5$ for electron-phonon scattering, respectively. This rather unusual temperature exponent is commonly attributed to a phonon-assisted s-d interband scattering.

High-pressure synchrotron x-ray diffraction (XRD) measurement is conducted to check the structural stability of the $2H_a$-MoS$_2$. The XRD patterns (run 1) from ambient
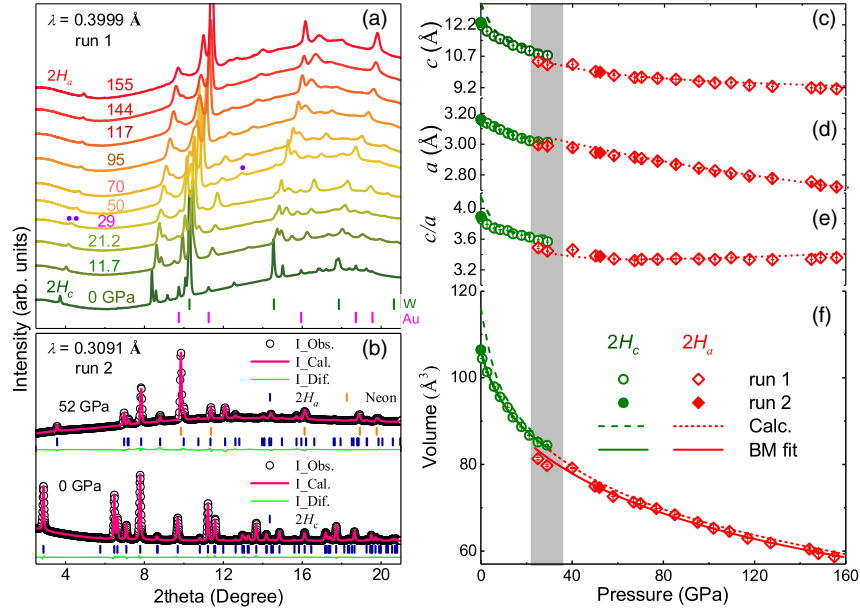
FIG. 4.   High-pressure synchrotron x-ray diffraction analysis of $2H$-MoS$_2$. (a) XRD patterns from ambient pressure up to 155 GPa at room temperature (run 1, $\lambda = 0.3999$ Å). (b) Rietveld refinements on XRD patterns of the $2H_c$ phase at 0 GPa and the $2H_a$ phase at 52 GPa (run 2, $\lambda = 0.3091$ Å). (c)–(f) Pressure dependence of experimental and calculated lattice constant c, lattice constant a, axial ratio c/a and unit-cell volume. The solid line represents the fitting of experimental P-V data by the Birch-Murnaghan equation of state.

pressure up to 155 GPa are shown in Fig. 4(a). Rietveld refinements on the XRD patterns (run 1) at ambient pressure, 50 and 155 GPa are given in Fig. S2 [25]. For the XRD pattern at 29 GPa, the subtle change of the diffraction peak at the low angle of ~4° corresponding to the $2H_c$-to-$2H_a$ polytype transformation via interlayer sliding is consistent with our previous XRD study [23]. As shown in Fig. S3 [25], the coordinate of the S atom is the same for these two polytypes, but the Mo atom occupies the $2b$ (0, 0, 0.25) site in the $2H_a$ phase and the $2c$ (1/3, 2/3, 0.25) site in the $2H_c$ phase, respectively. This polytype transformation is completed at ca. 40 GPa. Upon further increasing the pressure to 155 GPa, there is no further change in the XRD patterns, confirming that the $2H_a$ phase is stable over the investigated pressure range. Rietveld refinements on the XRD patterns (run 2) at ambient pressure for the $2H_c$ phase and at 52 GPa for the $2H_a$ phase are shown in Fig. 4(b). The obtained lattice constants and Wyckoff position of the S atom are $a = 3.1618(1)$ Å, $c = 12.3043(4)$ Å, and $4f$ (1/3, 2/3, 0.622) at ambient pressure, and $a = 2.9442(1)$ Å, $c = 9.941(2)$ Å, and $4f$ (1/3, 2/3, 0.085) at 52 GPa, respectively. The detailed results of the Rietveld refinements are listed in Table S1. The structural stability of the $2H_a$ phase is further substantiated by *in situ* high-pressure Raman measurement at room temperature during the electrical transport measurements, as shown in Fig. S4 [25]. From both experiments, it is concluded that the $2H_a$-MoS$_2$ is quite robust against pressure without any structural phase transition, decomposition and amorphization up to 155 GPa. These

results help confirm that the observed superconductivity is an intrinsic property of the $2H_a$-MoS$_2$. The experimental and calculated pressure-dependent lattice constants, axial ratio and unit-cell volume are plotted in Figs. 4(c)–4(f), respectively. Fitting the experimental P-V data with the Birch−Murnaghan equation of state [45] yields the following bulk modulus B_0 and unit cell volume V_0, i.e., $B_0 = 50(12)$ GPa, $V_0 = 106.3(11)$ Å^3 for the $2H_c$ phase and $B_0 = 110(7)$ GPa, $V_0 = 98(1)$ Å^3 for the $2H_a$ phase, respectively. The volume collapse at the polytype transformation is ca. 4%. The pressure-dependent in-plane and out-of-plane lattice contraction is shown in Fig. S5 [25]. The out-of-plane lattice contraction c/c_0 is larger than the in-plane lattice contraction a/a_0 for both phases, reflecting the anisotropic compressibility due to weak van der Waals interlayer bonding and strong covalent intralayer bonding.

The observed T_c is orders of magnitude higher than the BCS value estimated via the Allen-Dynes formula with an electron-phonon coupling (EPC) strength λ of 0.11 at 100 GPa [46]. Interestingly, Kohulak *et al.* predicted a $P4_1/mmm$ phase with a λ of 0.75 corresponding to a superconducting T_c of 15 K [47]. To understand the observed superconductivity in the $2H_a$ phase, density functional theory (DFT) calculations [25] are performed to examine the evolution of band structure and Fermi surface with pressure. The calculated band structure (Fig. S6 [25]) and Fermi surface (Fig. S7 [25]) indicate that a flat hole-type Fermi pocket emerges around the H-K high-symmetry line in the electronic structure at 150 GPa compared to that at 80 GPa. We speculate that this new

Fermi pocket plays a key role in facilitating the emergence of superconductivity.

CDW is a well-defined electronic ground state that competes with superconductivity in TMDs with the exception of $2H$-NbS$_2$. Very recently, the phonon-mediated superconductivity in $2H$-NbS$_2$ was demonstrated to be intimately linked to the Fermi surface arcs exhibiting an exceptionally strong electron-phonon interaction. The electron-lattice coupling is dictated by the low-energy anharmonic phonon modes, which drives the system to be on the verge of a latent CDW instability [48]. The hump in the $R(T)$ at 30 GPa, evident in Fig. 1(a), might be a signature of CDW driven by an excitonic insulator phase [49]. Such a CDW presumably intervenes prior to the closure of the band gap and the pressure-induced "quantum melting" of CDW should be responsible for the observed superconductivity, as seen in $1T$-TiSe$_2$ [18] and $1T$-TaS$_2$ [19]. CDW in the electrostatically gated $2H_c$-MoS$_2$ driven by the softening of an acoustic phonon mode has been predicted [50]. However, the definitive evidence for pressure-induced CDW in $2H_a$-MoS$_2$ remains absent so far.

Upon electrostatic gating, superconductivity in the $2H_c$-MoS$_2$ emerges near either the $K(K')$ valleys or the $Q(Q')$ valleys of the conduction band. The Cooper pairs are formed by electrons at either the K point or the Q point [4]. The EPC strength λ and electronic DOS around the K point and the Q point are different [14]. At either point, electron feels a large SOC and in-plane effective magnetic field which renders a unique temperature dependence of the upper critical field. Both conventional phonon-mediated s-wave pairing superconductivity and unconventional superconductivity with opposite pairing signs for the electrons near opposite K points induced by the competition between electron-electron interaction and quasiparticle-phonon coupling in the electrostatically gated $2H_c$-MoS$_2$ have been proposed [51–53]. Because of the presence of a strong gating electric field which could break the inversion symmetry and mirror symmetry, Rashba SOC, which induces new superconducting phases beyond the conventional s-wave pairing and the spin-triplet s-wave-like pairing, can arise in the $2H_c$-MoS$_2$ [54]. Particularly, the spin-singlet p-wave-like phase, which breaks the time-reversal symmetry, is a promising candidate of topological superconductor. Also, a spin-triplet p-wave phase which can be stabilized by Rashba SOC is predicted to be in the topologically trivial regime in the electrostatically gated $2H_c$-MoS$_2$ [55].

Compared to electrostatic gating, the application of pressure acts by shifting both the valence and conduction bands to increase their overlap in energy which pushes the Fermi level further into both bands. For the $2H_c$-MoS$_2$, the resulting modification of the band structure is characterized by a progressive reduction of the indirect band gap between the Γ point and the Q point; this is also accompanied with a reduction of the in-plane effective mass and appearance of straight bands near the Γ point and the K point at the Fermi

level. At a sufficient pressure, Dirac conelike structures appear at the Γ point [56]. Our DFT calculations show that two Fermi pockets around the H-K and the Γ-A high-symmetry lines coexist at 150 GPa. We conjecture that the concurrence of these two Fermi pockets is closely related to the emergence of superconductivity. Hence, the origin of superconductivity achieved via pressure is different from that achieved via electrostatic gating, at least from the viewpoint of electronic structure.

In conclusion, the $2H_c$-MoS$_2$ undergoes a pressure-induced $2H_c$-to-$2H_a$ polytype transformation near 30 GPa accompanied with a semiconductor-to-metal transition. The $2H_a$ phase is confirmed to be stable up to 155 GPa, and exhibits superconductivity at pressures starting from above 90 GPa. The superconducting T_c increases quickly from $\sim$5 K at 100 GPa to $\sim$12 K at 120 GPa, and remains nearly constant over a broad pressure range up to 220 GPa. Our present finding represents the first experimental realization of pressure-induced superconductivity with a record-high T_c of 12 K in a pristine CDW-free $2H$ polymorph of TMDs.

---

[*]liyc@ihep.ac.cn
[†]zhaojg@hit.edu.cn
[‡]zryang@issp.ac.cn

[1] B. Radisavljevic, A. Radenovic, J. Brivio, V. Giacometti, and A. Kis, Nat. Nanotechnol. **6**, 147 (2011).

[2] K. F. Mak, K. He, J. Shan, and T. F. Heinz, Nat. Nanotechnol. **7**, 494 (2012).

[3] X. F. Qian, J. W. Liu, L. Fu, and J. Li, Science **346**, 1344 (2014).

[4] J. M. Lu, O. Zheliuk, I. Leermakers, N. F. Q. Yua, U. Zeitler, K. T. Law, and J. T. Ye, Science **350**, 1353 (2015).

[5] M. Chhowalla, H. S. Shin, G. Eda, L-J. Li, K. P. Loh, and H. Zhang, Nat. Chem. **5**, 263 (2013).

[6] Q. H. Wang, K. Kalantar-Zadeh, A. Kis, J. N. Coleman, and M. S. Strano, Nat. Nanotechnol. **7**, 699 (2012).

[7] Y. P. Qi *et al.*, Nat. Commun. **7**, 11038 (2016).

[8] R. B. Somoano and A. Rembaum, Phys. Rev. Lett. **27**, 402 (1971).

[9] E. Morosan, H. W. Zandbergen, B. S. Dennis, J. W. G. Bos, Y. Onose, T. Klimczuk, A. P. Ramirez, N. P. Ong, and R. J. Cava, Nat. Phys. **2**, 544 (2006).

[10] K. E. Wagner, E. Morosan, Y. S. Hor, J. Tao, Y. Zhu, T. Sanders, T. M. McQueen, H. W. Zandbergen, A. J. Williams, D. V. West, and R. J. Cava, Phys. Rev. B **78**, 104520 (2008).

[11] L. J. Li, E. C. T. O'Farrell, K. P. Loh, G. Eda, B. Ozyilmaz, and A. H. Castro Nature (London) **529**, 185 (2016).

[12] Y. J. Yu *et al.*, Nat. Nanotechnol. **10**, 270 (2015).

[13] J. T. Ye, Y. J. Zhang, R. Akashi, M. S. Bahramy, R. Arita, and Y. Iwasa, Science **338**, 1193 (2012).

[14] D. Costanzo, S. Jo, H. Berger, and A. F. Morpurgo, Nat. Nanotechnol. **11**, 339 (2016).

[15] V. D. Blank and E. I. Estrin *Phase Transitions in Solids Under High Pressure* (CRC Press, Taylor & Francis, New York, 2014).

[16] V. Panchal, D. Errandonea, A. Segura, P. Rodriguez-Hernandez, A. Munoz, S. Lopez-Moreno, and M. Bettinelli, J. Appl. Phys. **110**, 043723 (2011).

[17] D. Errandonea, E. Bandiello, A. Segura, J. J. Hamlin, M. B. Maple, P. Rodriguez-Hernandez, and A. Munoz, J. Alloys Compd. **587**, 14 (2014).

[18] A. F. Kusmartseva, B. Sipos, H. Berger, L. Forro, and E. Tutis, Phys. Rev. Lett. **103**, 236401 (2009).

[19] B. Sipos, A. F. Kusmartseva, A. Akrap, H. Berger, L. Forro, and E. Tutis, Nat. Mater. **7**, 960 (2008).

[20] D. F. Kang *et al.*, Nat. Commun. **6**, 7804 (2015).

[21] X. C. Pan *et al.*, Nat. Commun. **6**, 7805 (2015).

[22] A. P. Nayak, S. Bhattacharyya, J. Zhu, J. Liu, X. Wu, T. Pandey, C. Q. Jin, A. K. Singh, D. Akiwande, and J-F. Lin, Nat. Commun. **5**, 3731 (2014).

[23] Z. H. Chi, X. M. Zhao, H. D. Zhang, A. F. Goncharov, S. S. Lobanov, T. Kagayama, M. Sakata, and X. J. Chen, Phys. Rev. Lett. **113**, 036802 (2014).

[24] Y. J. Zhang, J. T. Ye, Y. Yomogida, T. Takenobu, and Y. Iwasa, Nano Lett. **13**, 3023 (2013).

[25] See Supplemental Material at http://link.aps.org/supplemental/10.1103/PhysRevLett.120.037002 for the experimental and calculation details and the supporting results, which includes Refs. [26–34].

[26] H.-K. Mao, J. Xu, and P. M. Bell, J. Geophys. Res. **91**, 4673 (1986).

[27] Y. Akahama and H. Kawamura, J. Appl. Phys. **96**, 3748 (2004).

[28] A. P. Hammersley, S. O. Svensson, M. Hanfland, A. N. Fitch, and D. Hausermann, High Press. Res. **14**, 235 (1996).

[29] Y. Wang, J. Lv, L. Zhu, and Y. Ma, Phys. Rev. B **82**, 094116 (2010).

[30] Y. Wang, J. Lv, L. Zhu, and Y. Ma, Comput. Phys. Commun. **183**, 2063 (2012).

[31] J. P. Perdew, K. Burke, and M. Ernzerhof, Phys. Rev. Lett. **77**, 3865 (1996).

[32] P. E. Blöchl, Phys. Rev. B **50**, 17953 (1994).

[33] J. Klimeš, D. R. Bowler, and A. Michaelides, Phys. Rev. B **83**, 195131 (2011).

[34] N. Troullier and J. L. Martins, Phys. Rev. B **43**, 1993 (1991).

[35] D. Errandonea, Y. Meng, M. Somayazulu, and D. Hausermann, Physica (Amsterdam) **355B**, 116 (2005).

[36] D. Errandonea, A. Munoz, and J. Gonzalez-Platas, J. Appl. Phys. **115**, 216101 (2014).

[37] N. R. Werthamer, E. Helfand, and P. C. Hohenberg, Phys. Rev. **147**, 295 (1966).

[38] J. A. Woollam, R. B. Somoano, and P. O. Connor, Phys. Rev. Lett. **32**, 712 (1974).

[39] I. Guillamon, H. Suderow, S. Vieira, L. Cario, P. Diener, and P. Rodiere, Phys. Rev. Lett. **101**, 166407 (2008).

[40] T. Yokoya, T. Kiss, A. Chainani, S. Shin, M. Nohara, and H. Takagi, Science **294**, 2518 (2001).

[41] P. Szabo, P. Samuely, J. Kacmarcik, T. Klein, J. Marcus, D. Fruchart, S. Miraglia, C. Marcenat, and A. G. M. Jansen, Phys. Rev. Lett. **87**, 137005 (2001).

[42] K. Kirshenbaum, P. S. Syers, A. P. Hope, N. P. Butch, J. R. Jeffries, S. T. Weir, J. J. Hamlin, M. B. Maple, Y. K. Vohra, and J. Paglione, Phys. Rev. Lett. **111**, 087001 (2013).

[43] J. Bardeen, L. N. Cooper, and J. R. Schrieffer, Phys. Rev. **106**, 162 (1957); **108**, 1175 (1957).

[44] W. L. McMillan, Phys. Rev. **167**, 331 (1968).

[45] F. Birch, Phys. Rev. **71**, 809 (1947).

[46] L. Hromadova, R. Martonak, and E. Tosatti, Phys. Rev. B **87**, 144105 (2013).

[47] O. Kohulak, R. Martonak, and E. Tosatti, Phys. Rev. B **91**, 144113 (2015).

[48] C. Heil, S. Ponce, H. Lambert, M. Schlipf, E. R. Margine, and F. Giustino, Phys. Rev. Lett. **119**, 087003 (2017).

[49] H. Cercellier *et al.*, Phys. Rev. Lett. **99**, 146403 (2007).

[50] M. Rosner, S. Haas, and T. O. Wehling, Phys. Rev. B **90**, 245105 (2014).

[51] Y. Z. Ge and A. Y. Liu, Phys. Rev. B **87**, 241408(R) (2013).

[52] R. Roldan, E. Cappelluti, and F. Guinea, Phys. Rev. B **88**, 054515 (2013).

[53] T. Das and K. Dolui, Phys. Rev. B **91**, 094510 (2015).

[54] A. Kormanyos, V. Zolyomi, N. D. Drummond, and G. Burkard, Phys. Rev. X **4**, 011034 (2014).

[55] N. F. Q. Yuan, K. F. Mak, and K. T. Law, Phys. Rev. Lett. **113**, 097001 (2014).

[56] C. Espejo, T. Rangel, A. H. Romero, X. Gonze, and G.-M. Rignanese, Phys. Rev. B **87**, 245114 (2013).